Colorimetric Pressure Sensing by Plasmonic Decoupling of Silver

Nanoparticles Confined within Polymeric Nanoshells

Chen Chen, Qingsong Fan, Zhiwei Li, Zepeng Cai, Zuyang Ye, Yadong Yin*

Department of Chemistry, University of California, Riverside, California 92521, United States

*Email: yadong.yin@ucr.edu

Abstract

Employing a plasmonic decoupling mechanism, we report the design of a colorimetric pressure

sensor that can respond to applied pressure with instant color changes. The sensor consists of a

thin film of stacked uniform resorcinol-formaldehyde nanoshells with their inner surfaces

functionalized with silver nanoparticles. Upon compression, the flexible polymer nanoshells

expand laterally, inducing plasmonic decoupling between neighboring silver nanoparticles and a

subsequent blueshift. The initial color of the sensor is determined by the extent of plasmonic

coupling, which can be controlled by tuning the interparticle distance through a seeded growth

process. The sensing range can be conveniently customized by controlling the polymer shell

thickness or incorporating the hybrid nanoshells into various polymer matrices. The new

colorimetric pressure sensors are easy to fabricate and highly versatile, allow for convenient tuning

of the sensing range, and feature significant color shifts, holding great promise for a wide range of

practical applications.

KEYWORDS: silver nanoparticles, plasmonic decoupling, colorimetric pressure sensor,

deformation, polymer nanoshells

Pressure sensors are capable of transforming mechanical forces, such as tensile, compressive, and bending stresses, into discernible outputs.^{1–4} Conventional pressure sensors are electronic devices that can respond to mechanical forces with changes in their electrical properties, such as resistivity and capacitance.⁵ While they have many advantages, their adoption for applications is often hindered by structural rigidity and the need for power sources and external signal readers. To this end, colorimetric pressure sensors have gained attention due to their ability to provide observable optical responses.^{6–8} In contrast to electronic devices, colorimetric sensors exhibit high mechanical flexibility, allowing them to adapt to various surfaces.⁹ Typical colorimetric pressure sensors mainly operate based on stimuli-responsive changes in the lattice parameters and/or refractive indices of photonic crystals.^{10–12} Their large-scale applications are often challenged by the requirement of highly ordered structures, which involve complicated fabrication processes and high production costs. Additionally, the angular dependence of diffraction increases the complexity of interpreting signals in practical settings.

Noble metal nanoparticles (NPs) such as Au, Ag, and Cu are known for exhibiting unique optical properties owing to their strong localized surface plasmon resonance^{13,14}, which makes them highly interesting for sensing and imaging applications.^{6,15,16} In addition to their strong shape dependence, the resonance properties of the plasmonic nanoparticles are significantly affected by their surroundings.^{17,18} In particular, the resonance wavelength undergoes a significant red-shift when a nanoparticle is approached by others to a distance below approximately one diameter's length. The phenomenon known as plasmonic coupling, along with its counterpart, decoupling, gives rise to notable optical shifts that can be effectively influenced by precise control over

interparticle distances, offering a versatile tool for designing colorimetric sensors with tailored functionalities. 15,19

Here we present the design of a pressure sensor that can effectively respond to pressure changes by producing optical shifts based on plasmonic decoupling. The key components are polymer nanoshells synthesized with their inner surfaces functionalized with AgNPs through a templating approach. A robust seeded growth process is used to grow AgNPs and reduce their average interparticle distance, inducing significant plasmonic coupling that shifts the scattering into the longer wavelength of the visible spectrum. The application of compressive pressure triggers the lateral expansion of the hybrid nanoshells, resulting in the plasmonic decoupling of AgNPs and a subsequent visible optical blueshift. Among plasmonic metals, Ag is chosen for colorimetric sensing due to its nanoparticles' high plasmonic activity, appropriate resonance wavelength, good chemical stability, and easy synthesis via seed-mediated processes.²⁰ The thickness of the nanoshells and the inter-nanoparticle distances can be tailored to control the pressure-sensing thresholds to allow the detection of both high and low pressures. Furthermore, confining AgNPs within polymer shells provides significant flexibility in customizing pressure sensors to meet specific requirements such as sensing range and surface adhesion, as the hybrid nanostructures can be easily integrated into various polymer matrices without concerns about the chemical compatibility between AgNPs and the matrix materials. The pressure sensor is easy to fabricate, highly versatile and customizable, and has high sensitivity and a broad sensing range, making it ideal for various pressure detection applications.

The hybrid nanoshells were fabricated by combining a templating process to create the polymer shells and then a seeded growth process to introduce AgNPs to their inner surfaces, as schematically shown in Figure 1a.^{21–24} Specifically, SiO₂ nanospheres were synthesized using a Stöber method and then utilized as the primary templates for creating the polymer shells (Figure 1b). The SiO₂ surface was then modified by 3-aminopropyltriethoxysilane (APTES), followed by the attachment of Au seeds (Au-s) through the coordinate interactions between Au atoms and amino groups (Figure 1c). The resulting particles were overcoated with a resorcinol-formaldehyde (RF) layer through a sol-gel-like process (Figure 1d), ²⁵ producing SiO₂@Au-s@RF core-shell particles. Similar to sol-gel-derived colloidal SiO₂, the as-prepared RF shells feature micropores that allow the diffusion of water molecules and precursor ions. Therefore, selective deposition of metallic Ag on the Au seeds could be achieved in the limited space sandwiched between the SiO₂ core and RF shell by reducing the Ag precursors by formaldehyde in the SiO2@Au-s@RF dispersion (Figure 1e).²⁶ As one of its major advantages, the seeded growth process allows the precise control of the size of the resulting AgNPs and the interparticle distances. Finally, removing SiO₂ templates with hydrofluoric acid (HF) produced hybrid nanoshells with AgNPs retained on the inner surfaces. Figure 1f showcases a representative sample of hybrid nanoshells, denoted as S-40 to reflect their shell thickness of 40 nm. The illustration highlights a consistently uniform and smooth shell structure featuring an average cavity diameter of 200 nm. In contrast to initial SiO₂ cores containing only Au seeds, there is a noticeable reduction in the interparticle distance among AgNPs, resulting in a significant enhancement of plasmonic coupling, as discussed in more detail in the next section.

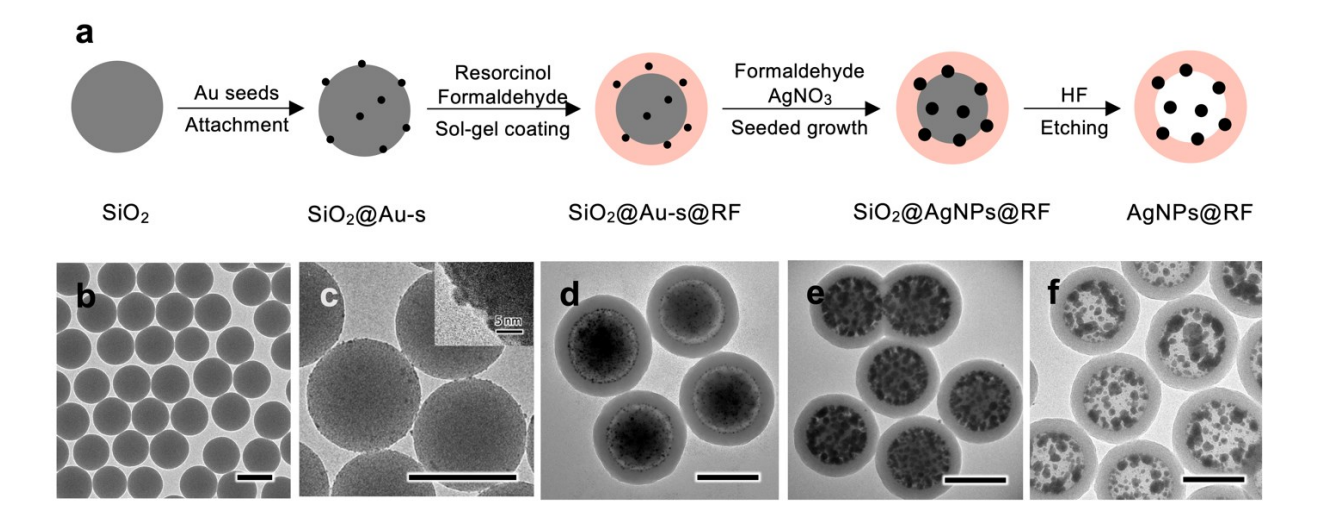


Figure 1. Synthesis of polymeric nanoshells with their inner surface decorated with AgNPs. (a) Schematic representation of the synthesis of AgNPs@RF nanoshells; (b-f) TEM images of SiO₂ spheres (b); SiO₂@Au-s spheres (c), with the inset showing the magnified image of sphere surface; SiO₂@Au-s@RF spheres (d); SiO₂@AgNPs@RF spheres (e); AgNPs@RF nanoshells (f). The scale bars are 200 nm.

Pressure-sensing films were prepared by drop-casting an ethanol dispersion of AgNPs@RF nanoshells on a plastic sheet. The hybrid nanoshells retained their hollow morphology during rapid ethanol evaporation, as illustrated in Figure 2d. The resulting film exhibited a dark brown appearance, attributed to the absorption of RF shells and the plasmonic resonance of AgNPs.

The pressure-sensing capability of the colorimetric films was assessed using a hydraulic press capable of displaying the applied force. The instantaneous pressure (P) was determined by dividing the applied force (F) by the contact surface area (A), represented as P = F/A. Applying relatively low pressure (50 MPa) for 5 seconds resulted in the film's color change from brown to light blue (Figure 2a-b). The plastic nature of the polymer shells ensured their irreversible deformation from

a spherical shape to an oblate shape under flat plate indentations. Uneven deformation, appearing as minute spots of different colors, is believed to result from the non-uniform propagation and distribution of the pressure applied within a short period.

With the pressure increasing to 80 MPa, the film color shifted to purple (Figure 2c). As depicted in Figure 2d-f, the compression induced a gradient lateral expansion and decreased the vertical diameter (Figure S1). Simultaneously, the interparticle distance of AgNPs increased through lateral expansion of the shells, as illustrated in Figure 2g. The irreversible deformation of the hollow shells enabled the film to memorize mechanical stress, as the colors and optical extinction profiles remained unchanged after a week or even longer at room temperature. In contrast to AgNPs@RF shells, pure RF shells displayed no apparent color response, regardless of the applied pressure, highlighting the crucial role of AgNPs for pressure sensing (Figure S2).

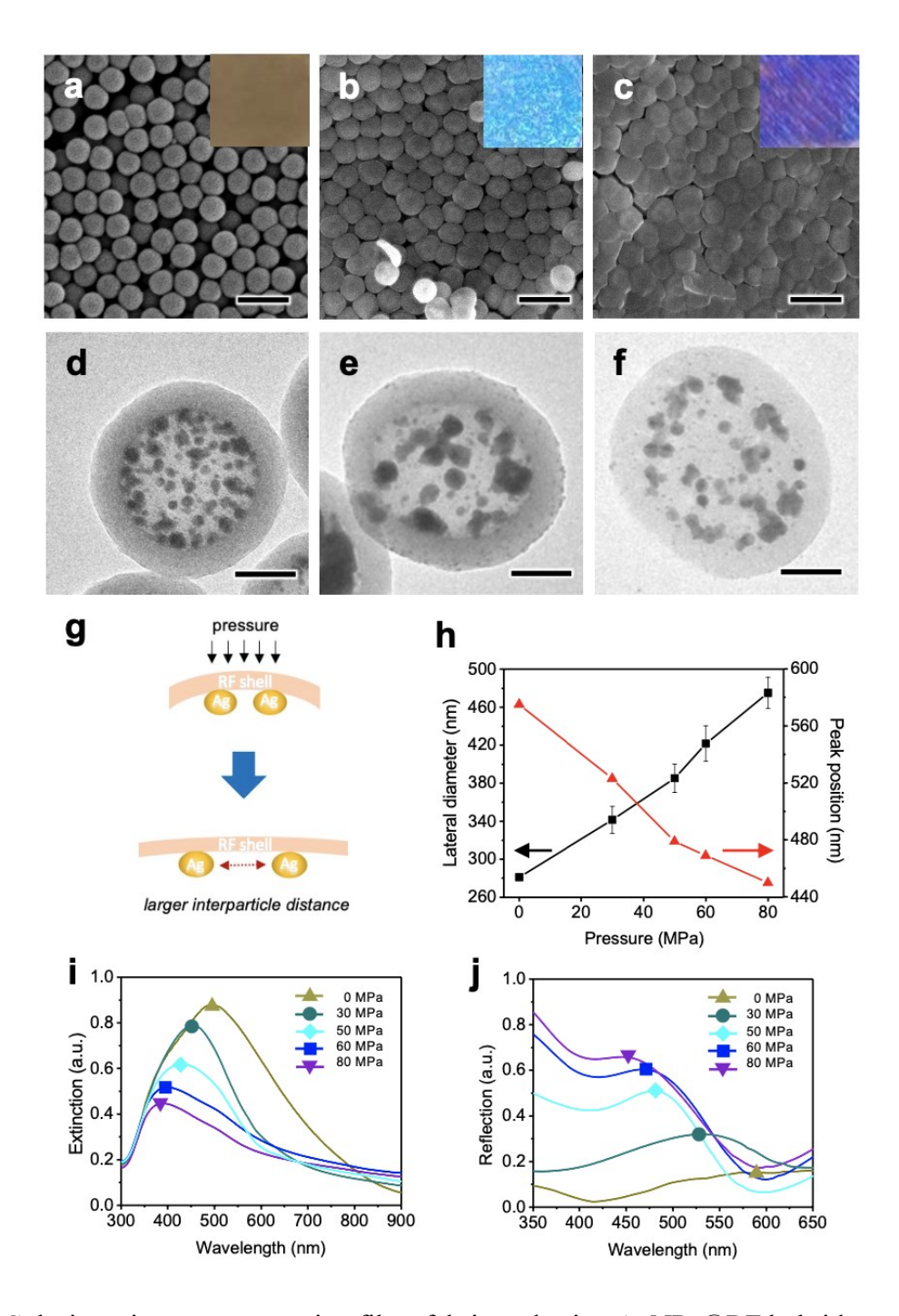


Figure 2. Colorimetric pressure-sensing films fabricated using AgNPs@RF hybrid nanoshells. (a-c) SEM image of sample S-40, compressed S-40 at 50 MPa and 80 MPa; (d-f) TEM images of sample S-40, compressed S-40 at 50 MPa and 80 MPa, respectively; (g) Schematic representation of the plasmonic decoupling in compression process; (h) Relationship between lateral expansion and reflected wavelength at different pressure; (i) Extinction spectra of sample S-40, compressed

S-40 at 30 MPa, 50 MPa, 60 MPa, and 80 MPa; (j) Reflectance spectra of sample S-40, compressed S-40 at 30 MPa, 50 MPa, 60 MPa, and 80 MPa. All the insets are digital photos of pressure-sensing films. The scale bars are 500 nm in SEM images and 100 nm in TEM images.

The unusual color change mainly results from reduced plasmonic coupling during the deformation of polymeric nanoshells. When AgNPs move away from each other, the increased interparticle distance allows the plasmon resonance to occur at a higher frequency, leading to a blueshift in the resonance wavelength.²⁷ Illustrated in Figure 2i, the UV-vis extinction spectra of the initial film display a broad peak at around 500 nm. This broad peak is attributed to the random distribution of AgNPs and indicates strong plasmonic coupling effect. The application of sufficient pressure caused the fusion of adjacent AgNPs, thus decreasing their number and reducing the plasmonic coupling effect. At the same time, the vertical compression of the spherical RF shells significantly expanded their lateral dimension, resulting in a larger average interparticle distance that led to the decoupling of the plasmonic resonance between neighboring AgNPs and, consequently, a continuous peak shift to a shorter wavelength of approximately 400 nm. As indicated in Figure 2h, the irreversible lateral expansion increased proportionally with the intensity of applied stress, resulting in a continuous color shift to changes in pressure (Figure S3). To better understand the optical properties, we have conducted simulations to calculate the extinction, scattering, and absorption of AgNPs@RF spheres under two extreme conditions, with the details depicted in the supporting information (Figure S4a-b). A similar blue-shift from a broad peak was observed upon compression, reflecting the decreasing plasmonic coupling among AgNPs (Figure S4c), which was consistent with our experimental observation. When AgNPs in compressed spheres were etched in a saturated NaCl solution²⁸, the color response almost disappeared, confirming the dominant

contribution from the plasmonic property of AgNPs (Figure S5). Furthermore, the plasmonic decoupling depends on the deformation of individual nanoshells rather than their interactions. Consequently, the film can exhibit a uniform color with high quality across the entire pressed area. This fabrication strategy of pressure sensors circumvents many limitations in conventional systems, such as self-assembled colloidal photonic crystals, providing possibilities in more complicated applications.

It is worth noting that the reflectance intensity of the film experienced a surprising enhancement after compression (Figure 2h). Prior to compression, the initial AgNPs were randomly distributed on the inner surface of the RF shells, resulting in omnidirectional light scattering. However, upon compression, the RF shells were converted into plates parallel to the substrate. The enclosed AgNPs also aligned laterally, thus enhancing the overall light-scattering intensity.

The size and interparticle distance of AgNPs can be manipulated by controlling the seeded growth process. Increasing the concentration of the Ag precursor allows more Ag atoms to be deposited on each Au seed, changing the absorption and scattering of the resulting AgNPs and, consequently, the film color from light orange to dark brown (Figure 3a-d). At the initial growth stage, the plasmonic peak at 520 nm was mainly attributed to the Au seeds attached to the RF surface (sample S-3a). The characteristic resonance peak of AgNPs at 425 nm appeared when their size was over 10 nm (sample S-3b). Continued deposition increased average particle sizes (to ~20 nm for sample S-3c and ~36 nm for sample S-3d, with broad size distribution) and reduced overall interparticle distances, red-shifting and broadening their plasmonic peaks (Figure 3i). When the film was compressed to cause the RF shells to expand laterally, the interparticle separation increased,

reducing the plasmonic coupling and inducing a blue-shift. As shown in Figures 3e-h, under the same pressure (50 MPa), S-3a only exhibited an insignificant color change, but samples S-3b to 3d demonstrated obvious high-contrast color changes that were consistent with their more dramatic blue-shift in the plasmonic peaks (Figure 3i, S6). It should be noted that too much Ag deposition led to the formation of nearly complete Ag shells (Figure S7a-b). In this case, the films directly changed from brown to light pink under a small pressure due to the formation of complete Ag nanoplates. Even if we kept increasing the force, they could not show any different color response due to the unchangeable interparticle distance. The occurrence of plate-shaped AgNPs limited the plasmonic decoupling process, which was not ideal for colorimetric sensing because of the narrow tuning range. (Figure S7c-f).

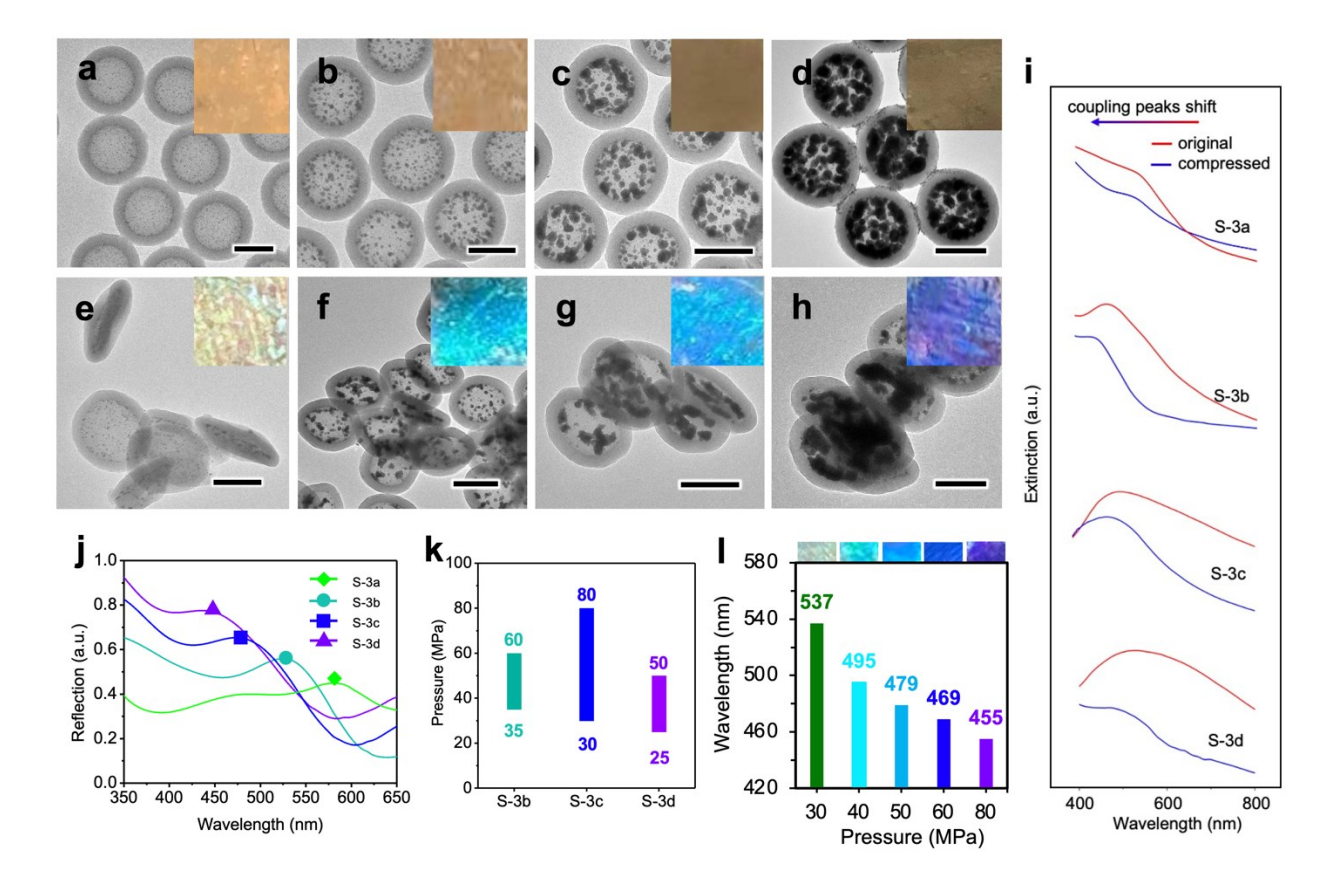


Figure 3. Seeded growth of AgNPs within polymer nanoshells. (a-d) TEM images of AgNPs@RF nanoshells with increased Ag deposition amount, named S-3a (a), S-3b (b), S-3c (c), S-3d (d); (e-

h) TEM images of compressed AgNPs@RF spheres from samples S-3a (e), S-3b (f), S-3c (g), and S-3d (h); (i) Extinction spectra of hollow and compressed samples; (j) Reflection spectra of compressed AgNPs@RF films; (k) Pressure-sensing thresholds for samples S-3b, S-3c, and S-3d; (l) Relationship between pressure and reflected wavelength of S-3c. The scale bar is 200 nm in TEM images. All the insets are digital photos of the pressure-sensing films.

While increasing Ag deposition enhances the reflection intensity of the compressed films (Figure 3j), it did not expand the detection range continuously. Here, we compared the films made from S-3b, S-3c, and S-3d to test their detection thresholds. The lower limit was stipulated as the minimum pressure required to show a significant color response, and the upper limit represented the maximum pressure that could induce a color response. The three films exhibited similar lower limits, only slightly decreasing with more Ag deposition. However, their maximum response pressures showed a marked difference (Figure 3k). While more Ag deposition generally benefited plasmonic coupling and more blue-shift upon compression, too much of it caused the fusion of the NPs from the top and bottom inner surfaces of the RF shells, producing anisotropic disk-shaped particles and red-shift. The combined effect resulted in no obvious color change for sample S-3d when applying relatively high pressure. Compared with the other two, sample S-3c with moderate Ag deposition exhibited the highest upper limit for pressure sensing, showing a continuous color shift when compressed under pressure from 30 to 80 MPa (Figure 31).

An extended pressure range is often desirable in many applications. Here, we show that the pressure response range of the sensing film can be conveniently extended by increasing the RF shell thickness during their sol-gel synthesis. In principle, the pressure-sensing threshold is

predominantly dictated by the deformation capacity of the shells or, conversely, by their stiffness.²⁹ The thin elastic shell deformation under compression follows non-linear Reissner's equation, with the shell stiffness (k_{shell}) determined by:

$$k_{shell} = \frac{4E_s h^2}{R\sqrt{3(1-\nu^2)}} \tag{1}$$

where E_s is Young's modulus, h is the shell thickness, R is the outer radius of the shell, and ν is Poisson's ratio.³⁰ For pure hollow RF shells with the same cross-linking degree, their E_s and ν remain constant. Since R is the sum of the inner radius of RF shells (r) and h, the relationship becomes:

$$k_{shell} \propto \frac{h^2}{r+h}$$
 (2)

Therefore, the stiffness of hollow shells mainly depends on RF thickness because the inner radius does not change under this condition. In brief, when the shell is thicker, the stiffness is larger, leading to a lower limit for deformation in pressure sensing.

The theoretical understanding was confirmed experimentally with the estimated shell stiffness of sample S-40. Generally, stiffness is a measure of the ability to resist deformation when subjected to an applied force, and in this case, it relates to the minimum threshold of color response. Therefore, we first used the inner radius and shell thickness of sample S-40 and its lower sensing limit to determine the shell stiffness constant in Reissner's equation (Supporting information, Calculation 1). Subsequently, three new samples were fabricated with different RF thicknesses: 47 nm (S-47), 55 nm (S-55), and 70 nm (S-70) (Figure 4a-c). By inputting the specific parameters of

the samples and shell stiffness constants into the Reissner equation, we were able to predict their minimum response pressures at 39 MPa, 51 MPa, and 76 MPa, respectively. As expected, when Ag was deposited in moderation, all the films showed continuous blue-shift in color under an increasing force with the occurrence of lateral expansion (Figure S8). Their lower limits were 40 MPa, 50 MPa, 75 MPa, respectively, which were consistent with our calculations (Figure 4e-g). Compared to S-40, samples S-47, S-55, and S-70 required markedly increased pressure to show the same response color (Figure 4d). Moreover, estimating the upper limits of the three samples by Reissner's theory suggested the maximum pressures of 105 MPa, 137 MPa, and 202 MPa, respectively (Supporting information Calculation 2), which were also close to the measured upper limits of the pressure thresholds (Figure 4h). Analyses of the three samples show percent errors smaller than 5%, confirming the high accuracy of the pressure sensing films (Table S2). The remarkable alignment observed between theoretical predictions and experimental outcomes serves as a robust validation for the dependability of designing a variety of pressure sensors utilizing our hollow hybrid nanoshells. By exploiting the relation between shell thickness and sensing threshold, we can tailor the design of pressure sensors to specific application conditions and achieve a targeted threshold for optimal performance.

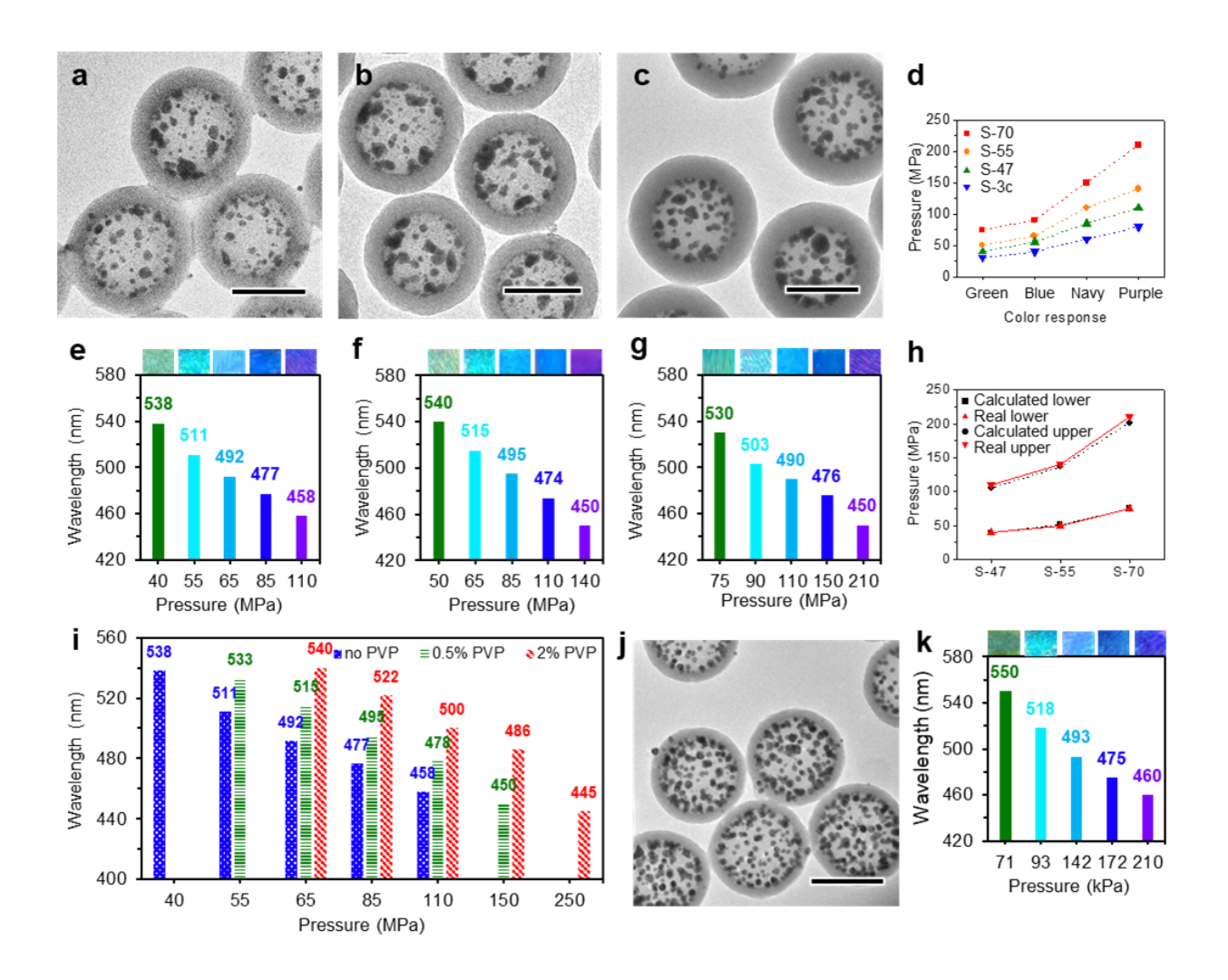


Figure 4. Tuning sensing threshold by controlling polymer shell thickness. (a-c) TEM images of AgNPs@RF nanoshells with different RF thicknesses, named S-47 (a), S-55 (b), and S-70 (c); (d) Required pressure to show response colors for samples S-40, S-47, S-55, and S-70; (e-g) Relationships between pressure and reflected wavelength of samples S-47 (e), S-55 (f), and S-70 (g), with the insets on top showing digital photos of the sensing films at different pressure; (h) Comparisons of calculated and real thresholds for samples S-47, S-55, and S-70; (i) Dependence of pressure sensing threshold of films prepared by drying sample S-40 with different amounts of PVP; (j) TEM image of AgNPs@RF nanoshells with a 25-nm shell, named S-25; (k) Relationships

between pressure and reflected wavelength of samples S-25. The scale bars in the TEM images are 200 nm.

The upper limit of pressure sensing can be further enhanced by tuning the rigidity of the film with additional polymers. For example, we demonstrate that polyvinylpyrrolidone (PVP) can be introduced into the colloidal dispersion of the hybrid nanoshells and enhance the rigidity of the resulting sensing film. As shown in Figure 4i, the film prepared with the addition of 0.5 wt% PVP solution shifted the sensing threshold to a higher value than the one without, while the one with 2 wt% PVP solution exhibited a more pronounced effect, increasing the upper limit to 250 MPa. These results confirm that creating composite films with varying rigidities is a sound approach for further enhancing the sensing range, which is important in substantially broadening the scope of real-world applications.

The thickness of the RF shells can also be reduced to increase film sensitivity to low pressure to meet the requirements of specific applications. Figure 4j shows a TEM image of AgNPs@RF particles with a 25-nm shell. As the film exhibited a response much lower than the detection threshold of the hydraulic press, a tubular impact tester was used to detect the small pressure. The falling weight accelerated until it hit the mount, creating a color response in the composite film due to the impulse. The hitting moment, captured by a high-speed camera, was used to estimate the instant pressure (see the detailed calculation in Supporting Information Calculation 3). Compared to previous samples, a thinner shell drastically reduced the pressure threshold. The color response occurred at only 71 kPa, almost 400 times lower than S-40. A purple color response appeared at 210 kPa, reaching the upper limit of the pressure threshold (Figure 4k). The film could

even respond to human-induced pressure, demonstrated, for instance, by its reaction to impact from a rubber hammer (Figure S9). This remarkably enhanced sensitivity was attributed to the flexibility of the RF nanoshells. The film exhibited different color responses upon slight pressure changes, which suggested its excellent sensitivity. Such high sensitivity enhances the usefulness of the sensor films in various conditions by meeting the requirements of detecting high or low pressure.

In order to showcase the accessibility of our pressure sensor, we have loaded the hybrid nanoshells on various substrate surfaces such as cotton fabric, wood, aluminum, stainless steel, and zinc. As a result, all the sensor films showed visible color changes under different pressure levels (as shown in Figure S10). The success on both flexible and rigid surfaces proves the practicality of the asdesigned sensors.

In summary, we have developed a novel colorimetric pressure sensor by taking advantage of the plasmonic decoupling of AgNPs associated with the compression-induced lateral expansion of polymer shells. Upon compression, the AgNPs attached to the inner surface of the polymer nanoshells move away from each other along with the lateral expansion of polymer shells, decreasing their plasmonic coupling and producing a color response depending on the deformation of RF shells. The design of the novel pressure sensor utilizes the unique properties of RF shells, including water and ion permeability, irreversible deformation, adjustable stiffness, and significant interaction with Au and Ag. In particular, the permeable nature of the RF shells enables controllable seeded growth of AgNPs on their inner surfaces, allowing facile control over the particle size and separation and, subsequently, the sensing threshold. The sensor films can be

fabricated to exhibit plasmonic color changes in response to a wide pressure range by controlling

the shell thickness or introducing additional polymers into the films. The simplicity of the

deposition process adds to the advantages of this colorimetric pressure sensor, enabling easy

coating on various substrates and demonstrating its versatility in different working environments.

Our pressure sensors feature easy fabrication, tunable thresholds, and high flexibility, offering

great potential to design novel colorimetric devices with exceptional sensing performance.

Supporting Information

The Supporting Information is available free of charge.

Additional experimental details, including methods, materials, preparation and

characterization of particles, simulation of plasmonic decoupling, calculation of sensing

thresholds, and quantification of pressure in impact tests (PDF).

Corresponding Author

Yadong Yin – Department of Chemistry, University of California, Riverside, California 92521,

United States; Email: yadong.yin@ucr.edu

Authors

Chen Chen – Department of Chemistry, University of California, Riverside, California 92521,

United States

Qingsong Fan – Department of Chemistry, University of California, Riverside, California 92521,

United States

Zhiwei Li – Department of Chemistry, University of California, Riverside, California 92521, United States

Zepeng Cai – Department of Chemistry, University of California, Riverside, California 92521, United States

Zuyang Ye – Department of Chemistry, University of California, Riverside, California 92521, United States

Author contributions

C.C. and Y.Y. conceived and planned this study. C.C. and Q.F. developed the methodology for modeling and simulation. C.C. and Z.L. developed the synthesis and characterization of nanoparticles. C.C. performed the pressure sensing measurements with the help of Z.C, and Z.Y. The manuscript was written through contributions of all authors. All authors discussed and analyzed the results and contributed to the writing of this paper.

Acknowledgements

The authors are grateful for the financial support from the U.S. National Science Foundation (CHE- 2203972).

Conflict of Interest

The authors declare no conflict of interest.

Data Availability Statement

The data that support the findings of this study are available from the corresponding author upon reasonable request.

References

- (1) Wang, H.; Zhou, R.; Li, D.; Zhang, L.; Ren, G.; Wang, L.; Liu, J.; Wang, D.; Tang, Z.; Lu, G.; Sun, G.; Yu, H. D.; Huang, W. High-Performance Foam-Shaped Strain Sensor Based on Carbon Nanotubes and Ti3C2TxMXene for the Monitoring of Human Activities. *ACS Nano* **2021**, *15* (6), 9690–9700.
- (2) Zhou, Z.; Chen, N.; Zhong, H.; Zhang, W.; Zhang, Y.; Yin, X.; He, B. Textile-Based Mechanical Sensors: A Review. *Materials* **2021**, *14*, 6073–6095.
- (3) Pasquale, M. Mechanical Sensors and Actuators. *Sens. Actuator A Phys.* **2003**, *106*, 142–148.
- (4) Parameswaran, C.; Gupta, D. Large Area Flexible Pressure/Strain Sensors and Arrays Using Nanomaterials and Printing Techniques. *Nano Converg.* **2019**, *6*, 28-51.
- (5) Jiao, P.; Egbe, K. J. I.; Xie, Y.; Nazar, A. M.; Alavi, A. H. Piezoelectric Sensing Techniques in Structural Health Monitoring: A State-of-the-Art Review. *Sensors* **2020**, *20* (13), 3730–3750.
- (6) Topcu, G.; Guner, T.; Inci, E.; Demir, M. M. Colorimetric and Plasmonic Pressure Sensors Based on Polyacrylamide/Au Nanoparticles. *Sens. Actuators A Phys.* **2019**, *295*, 503–511.
- (7) Snapp, P.; Kang, P.; Leem, J.; Nam, S. Colloidal Photonic Crystal Strain Sensor Integrated with Deformable Graphene Photo-Transducer. *Adv. Funct. Mater.* **2019**, *29* (33), 1902216.
- (8) Inci, E.; Topcu, G.; Guner, T.; Demirkurt, M.; Demir, M. M. Recent Developments of Colorimetric Mechanical Sensors Based on Polymer Composites. *J. Mater. Chem. C* **2020**, *8* (35), 12036–12053.
- (9) Piriya V.S, A.; Joseph, P.; Daniel S.C.G., K.; Lakshmanan, S.; Kinoshita, T.; Muthusamy, S. Colorimetric Sensors for Rapid Detection of Various Analytes. *Mater. Sci. Eng. C* **2017**, *78*, 1231–1245.

- (10) Ge J.; Yin Y. Responsive Photonic Crystal. Angew. Chem, Int. Ed. 2011, 50, 1492–1522.
- (11) Fu, Q.; Ge, J.; Chen, C.; Wang, Z.; Yang, F.; Yin, Y. High-Precision Colorimetric Sensing by Dynamic Tracking of Solvent Diffusion in Hollow-Sphere Photonic Crystals. *Research* **2022**, 2022, 1–11.
- (12) Jurewicz, I.; King, A. A. K.; Shanker, R.; Large, M. J.; Smith, R. J.; Maspero, R.; Ogilvie, S. P.; Scheerder, J.; Han, J.; Backes, C.; Razal, J. M.; Florescu, M.; Keddie, J. L.; Coleman, J. N.; Dalton, A. B. Mechanochromic and Thermochromic Sensors Based on Graphene Infused Polymer Opals. *Adv. Funct. Mater.* **2020**, *30* (31), 2002473.
- (13) Willets, K. A.; Van Duyne, R. P. Localized Surface Plasmon Resonance Spectroscopy and Sensing. *Annu. Rev. Phys. Chem.* **2007**, *58*, 267.–297.
- (14) Kristensen, A.; Yang, J. K. W.; Bozhevolnyi, S. I.; Link, S.; Nordlander, P.; Halas, N. J.; Mortensen, N. A. Plasmonic Colour Generation. *Nat. Rev. Mater.* **2016**, *2*, 16088.
- (15) Han X.; Liu Y.; Yin Y. Colorimetric Stress Memory Sensor Based on Disassembly of Gold Nanoparticle Chains. *Nano Lett.* **2014**, *14*, 2466–2470.
- (16) Choe, A.; Yeom, J.; Shanker, R.; Kim, M. P.; Kang, S.; Ko, H. Stretchable and Wearable Colorimetric Patches Based on Thermoresponsive Plasmonic Microgels Embedded in a Hydrogel Film. *NPG Asia Mater.* **2018**, *10* (9), 912–922.
- (17) González, A. L.; Noguez, C.; Beránek, J.; Barnard, A. S. Size, Shape, Stability, and Color of Plasmonic Silver Nanoparticles. *J. Phys. Chem. C* **2014**, *118* (17), 9128–9136.
- (18) Zhang, Q.; Li, N.; Goebl, J.; Lu, Z.; Yin, Y. A Systematic Study of the Synthesis of Silver Nanoplates: Is Citrate a "Magic" Reagent? *J. Am. Chem. Soc.* **2011**, *133* (46), 18931–18939.

- (19) Fu, L.; Liu, Y.; Wang, W.; Wang, M.; Bai, Y.; Chronister, E. L.; Zhen, L.; Yin, Y. A Pressure Sensor Based on the Orientational Dependence of Plasmonic Properties of Gold Nanorods. *Nanoscale* **2015**, *7* (34), 14483–14488.
- (20) Liu, X. Colloidal Plasmonic Nanoparticles for Ultrafast Optical Switching and Laser Pulse Generation. Front. Mater. 2018, 5 (59), 1-5.
- (21) Chen, J.; Feng, J.; Yang, F.; Aleisa, R.; Zhang, Q.; Yin, Y. Space-Confined Seeded Growth of Cu Nanorods with Strong Surface Plasmon Resonance for Photothermal Actuation. *Angew. Chem.* **2019**, *131* (27), 9376–9382.
- (22) Gao, C.; Zhang, Q.; Lu, Z.; Yin, Y. Templated Synthesis of Metal Nanorods in Silica Nanotubes. *J. Am. Chem. Soc.* **2011**, *133* (49), 19706–19709.
- (23) Chen, J.; Bai, Y.; Feng, J.; Yang, F.; Xu, P.; Wang, Z.; Zhang, Q.; Yin, Y. Anisotropic Seeded Growth of Ag Nanoplates Confined in Shape-Deformable Spaces. *Angew. Chem, Int. Ed.* **2021**, *60* (8), 4117–4124.
- (24) Chen, J.; Feng, J.; Li, Z.; Xu, P.; Wang, X.; Yin, W.; Wang, M.; Ge, X.; Yin, Y. Space-Confined Seeded Growth of Black Silver Nanostructures for Solar Steam Generation. *Nano Lett.* **2019**, *19* (1), 400–407.
- (25) Li, N.; Zhang, Q.; Liu, J.; Joo, J.; Lee, A.; Gan, Y.; Yin, Y. Sol-Gel Coating of Inorganic Nanostructures with Resorcinol-Formaldehyde Resin. *Chem. Commun.* **2013**, *49* (45), 5135–5137.
- (26) Li, Z.; Ye, Z.; Han, L.; Fan, Q.; Wu, C.; Ding, D.; Xin, H. L.; Myung, N. V.; Yin, Y. Polarization-Modulated Multidirectional Photothermal Actuators. *Adv. Mater.* **2021**, *33* (3), 2006367.
- (27) Hooshmand, N.; El-Sayed, M. Collective multipole oscillations direct the plasmonic coupling at the nanojunction interfaces. PNAS 2019, 116 (39), 19299-19304

- (28) Tran, V. T.; Lee, D. K.; Kim, J.; Lee, J.; Tufa, L. T.; Pham-Cong, D.; Kim, C. S.; Lee, J. Porosity-Controllable Magnetoplasmonic Nanoparticles and Their Assembled Arrays. *Nanoscale* **2020**, *12* (15), 8453–8465.
- (29) Zveryayev, Y. M. A Consistent Theory of Thin Elastic Shells. *J. Appl. Math. Mech.* **2016**, 80 (5), 409–420.
- (30) Walter, A.; Rehage, H.; Leonhard, H. Shear Induced Deformation of Microcapsules: Shape Oscillations and Membrane Folding. *Colloids Surf. A: Physicochem. Eng. Asp.* **2001**, *183*, 123–132.

For Table of Contents Only

